REPORT DOCUMENTATION PAGE

Form Approved
OMB No. 0704-0188

1. REPORT DATE	2. REPORT TYPE	3. DATES COVERED *(From - To)*
16 October 2020	Technical Paper	21 September 2020 - 19 October 2020

4. TITLE AND SUBTITLE
Experimental Methods for Solid Propellant Mechanical Behavior Characterization
(Project Title: Mechanical Properties of Solid Rocket Propellants at Shock Wave Rates)

5a. CONTRACT NUMBER

5b. GRANT NUMBER

5c. PROGRAM ELEMENT NUMBER

6. AUTHOR(S)
Dr. Sarah Bentil

5d. PROJECT NUMBER

5e. TASK NUMBER

5f. WORK UNIT NUMBER
Q16H

7. PERFORMING ORGANIZATION NAME(S) AND ADDRESS(ES)
Air Force Research Laboratory (AFMC)
AFRL/RQRP
10 E. Saturn Blvd.
Edwards AFB, CA 93524-7680

8. PERFORMING ORGANIZATION REPORT NUMBER

9. SPONSORING/MONITORING AGENCY NAME(S) AND ADDRESS(ES)

Air Force Research Laboratory (AFMC)
AFRL/RQR
5 Pollux Drive
Edwards AFB, CA 93524-7048

10. SPONSOR/MONITOR'S ACRONYM(S)

11. SPONSOR/MONITOR'S REPORT NUMBER(S)
AFRL-RQ-ED-TP-2020-204

12. DISTRIBUTION/AVAILABILITY STATEMENT
Distribution Statement A: Approved for Public Release; Distribution is Unlimited. PA Clearance Number: 20461 Clearance Date: 04 October 2020.

13. SUPPLEMENTARY NOTES
Summer Faculty Internship - End of term report. Prepared in collaboration with Iowa State University. The U.S. Government is joint author of the work and has the right to use, modify, reproduce, release, perform, display, or disclose the work.

14. ABSTRACT
Inert solid rocket propellant samples were subjected to dynamic inflation experiments, to characterize the high strain rate mechanistic response. During the experiments, an oxyacetylene-driven shock tube applied dynamic pressurization to the surface of the samples. Two high-speed cameras captured the deforming samples, which were speckled to measure the full-field surface displacements using the digital image correlation (DIC) algorithm. Concepts from both dynamic Kirchhoff plate bending theory and structural dynamics were used to mathematically derive the dynamic tensile elastic modulus, by considering both the initial transverse wave's phase velocity (transient response) and the vibration frequency (long-term response). An inverse finite element analysis (iFEA) was used to validate the mathematically derived tensile elastic modulus, by considering a linear elastic constitutive model. The calibrated tensile elastic modulus from the iFEA was comparable with the magnitude derived using the phase velocity. The iFEA was also used to characterize the linear viscoelastic (i.e. Prony series having either one or two Maxwell branches) behavior of the sample. The viscoelastic parameters calibrated using a Prony series with two Maxwell branches were in good agreement with the out-of-plane displacement data from DIC.

15. SUBJECT TERMS
N/A

16. SECURITY CLASSIFICATION OF: a. REPORT	b. ABSTRACT	c. THIS PAGE	17. LIMITATION OF ABSTRACT	18. NUMBER OF PAGES	19a. NAME OF RESPONSIBLE PERSON
					Timothy C. Miller
					19b. TELEPHONE NUMBER *(Include area code)*
Unclassified	Unclassified	Unclassified	SAR	16	N/A

Final Report

Research Opportunity
Experimental Methods for Solid Propellant Mechanical Behavior Characterization

Project Title: Mechanical Properties of Solid Rocket Propellants at Shock Wave Rates

AFRL Branch: AFRL/RQ-AFRL-Aerospace Systems
Advisor Name: Dr. Tim C. Miller
Principal Investigator: Sarah A. Bentil, Ph.D.

August 2020

Abstract

Inert solid rocket propellant samples were subjected to dynamic inflation experiments, to characterize the high strain rate mechanistic response. During the experiments, an oxyacetylene-driven shock tube applied dynamic pressurization to the surface of the samples. Two high-speed cameras captured the deforming samples, which were speckled to measure the full-field surface displacements using the digital image correlation (DIC) algorithm. Concepts from both dynamic Kirchhoff plate bending theory and structural dynamics were used to mathematically derive the dynamic tensile elastic modulus, by considering both the initial transverse wave's phase velocity (transient response) and the vibration frequency (long-term response). An inverse finite element analysis (iFEA) was used to validate the mathematically derived tensile elastic modulus, by considering a linear elastic constitutive model. The calibrated tensile elastic modulus from the iFEA was comparable with the magnitude derived using the phase velocity. The iFEA was also used to characterize the linear viscoelastic (i.e. Prony series having either one or two Maxwell branches) behavior of the sample. The viscoelastic parameters calibrated using a Prony series with two Maxwell branches were in good agreement with the out-of-plane displacement data from DIC.

1 Introduction

1.1 Motivation

Solid rocket propellants are comprised of a high-volume fraction of particles in a rubbery matrix material [15, 17, 23]. When debonding or dewetting of the particles occur, the solid rocket propellant becomes damaged [15, 23]. However, the high strain rate response of the damaged solid rocket propellants remains unknown. Thus, hindering the ability to effectively design sensors that can monitor the health of solid rocket propellants [10]. Consequently, the objective of this research opportunity is to couple digital image correlation (DIC) methods with shock tube experiments, to characterize the dynamic mechanical behavior of solid rocket propellants at high strain rates.

1.2 Background

Digital image correlation (DIC) is a non-contact optical method that has been widely applied in many areas of science and engineering for over 30 years [6, 21, 22]. Contactless measurements of soft deformable materials are important since minor disturbances on the material surface, due to strain gauge attachment, can influence the mechanical behavior [1, 2, 3, 14]. DIC is capable of quantifying both small and large deformation of soft materials at strain rates that range from quasistatic (10^{-6}/s – 10^{0}/s) to shock wave (10^{6}/s – 10^{8}/s) [3, 4, 5, 11, 12, 16, 18, 20, 24]. As a result, the DIC technique was applied to measure the three-dimensional (3D) full-field surface displacement of solid rocket propellants.

Inverse finite element analysis (iFEA) has been used in the literature to calibrate constitutive model parameters describing the mechanical properties of materials [7, 8]. During the iFEA, a comparison is made between the output from an experiment and simulated output following finite element simulations of the experiments. A match between the output implies that the mechanical properties of the material have been found. In this project, the iFEA was applied to determine the linear elastic and linear viscoelastic properties of HTPB samples exposed to a shock wave during a dynamic inflation experiment. Specifically, a comparison of calibrated constants using a Prony series, with either one or two Maxwell branches, was considered for the linear viscoelastic model.

2 Methods

2.1 Sample Preparation

Fifteen (15) solid rocket propellant samples were provided by Dr. Tim C. Miller (Senior Materials Research Engineer, U.S. Air Force Research Laboratory). The propellants were fabricated from the polymer matrix binder hydroxyl-terminated polybutadiene (HTPB), with aluminum as the fuel and ammonium perchlorate (AP) as the oxidizer. One (1) of the samples arrived having a circular plate (i.e. disc-shaped) geometry with a diameter of 152.4-mm (6-in.), to facilitate attachment with the end of the oxyacetylene-driven shock tube in Dr. Bentil's lab. The other fourteen (14) samples had a rectangular plate geometry with dimensions of 188-mm × 176-mm (7.4-in. × 6.9-in.), for ease during the sample preparation. Eight (8) of the fourteen (14) samples with the rectangular plate geometry were further cut into a circular plate (i.e. disc-shaped) geometry having a diameter of 152.4-mm (6-in.), once the samples were received by Dr. Bentil. All samples had a thickness of 5-mm (0.2-in.), to facilitate application of thin plate bending theory to characterize the mechanical behavior when assuming a linear elastic constitutive model. Table 1 highlights the geometric and material parameters for the HTPB samples, prior to the shock tube experiments. Details regarding why some samples, in Table 1, did not yield 3D–DIC data are explained in Section 3.1.

Table 1: *HTPB sample geometric and material parameters, along with samples containing 3D–DIC data.*

HTPB Sample Number	Geometry	Diameter (mm)	Length (mm)	Width (mm)	Thickness (mm)	Mass (g)	Volume (m^3)	Density (kg/m^3)	3D-DIC Data?
HTPB Sample 1	Disc	174.0			5.0	232.3	1.19E-04	1953.8	No
HTPB Sample 2	Rectangle	-	188.0	176.0	5.0	321.2	1.65E-04	1941.5	No
HTPB Sample 3	Rectangle	-	188.0	175.0	5.0	359.1	1.65E-04	2183.0	No
HTPB Sample 4	Rectangle	-	190.0	178.0	5.0	359.6	1.69E-04	2126.6	No
HTPB Sample 5	Rectangle	-	188.0	176.0	5.0	360.9	1.65E-04	2181.5	Yes
HTPB Sample 6	Rectangle	-	188.0	177.0	5.0	347.5	1.66E-04	2088.6	No
HTPB Sample 7	Rectangle	-	188.0	177.0	5.0	356.1	1.66E-04	2140.3	Yes
HTPB Sample 8	Disc	152.4	-	-	5.0	188.6	9.12E-05	2067.8	No
HTPB Sample 9	Disc	152.4	-	-	5.0	179.5	9.12E-05	1968.0	No
HTPB Sample 10	Disc	152.4	-	-	5.0	180.7	9.12E-05	1981.2	Yes
HTPB Sample 11	Disc	152.4	-	-	5.0	186.5	9.12E-05	2044.8	Yes
HTPB Sample 12	Disc	152.4	-	-	5.0	194.6	9.12E-05	2133.6	Yes
HTPB Sample 13	Disc	152.4	-	-	5.0	199	9.12E-05	2181.8	Yes
HTPB Sample 14	Disc	152.4	-	-	5.0	184.4	9.12E-05	2021.8	Yes
HTPB Sample 15	Disc	152.4	-	-	5.0	199.3	9.12E-05	2185.1	Yes

2.2 Shock tube Experiments

An oxyacetylene-driven shock tube was used to conduct the dynamic inflation experiments (Figure 1). The shock tube's driven section is instrumented with three (3) high frequency integrated circuit piezoelectric (ICP) pressure transducers (PCB Piezotronics, Model 102B15), to measure the speed of the shock wave and capture its pressure-time characteristics as a function of oxyacetylene volume in the driver section.

Each HTPB sample was speckled using flat white spray paint, to create the inherent speckle pattern needed for DIC analysis, prior to clamping at the end of the shock tube (Figure 2).

During the experiments, two synchronized high-speed digital cameras (Photron, FASTCAM SA-Z) with 105-mm macro lens (Nikon, AF-S VR Micro-NIKKOR 105-mm f/2.8G IF-ED) were used. The cameras were calibrated for stereovision prior to capturing images of the deforming propellant due to dynamic inflation following shock wave exposure. Images were acquired at a frame rate of 100,000 fps at a resolution of 640 $\times$ 280. The spatial resolution for images acquired during the oxyacetylene-driven shock tube experiments were 3 pixels/mm. Three-dimensional DIC analysis (3D–DIC) was performed using the commercially available VIC-3D (Correlated Solution) software, to quantify the 3D full-field surface deformation (i.e. displacement and strain) of HTPB. All tests were conducted at room temperature (21°C).

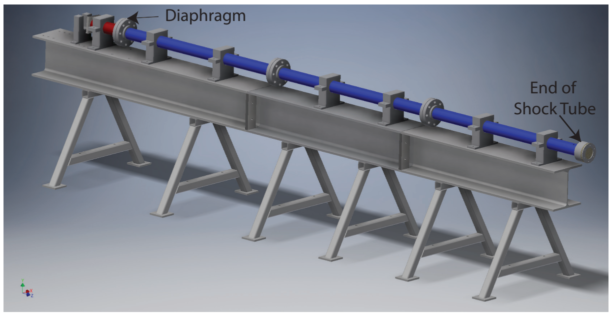

(a)

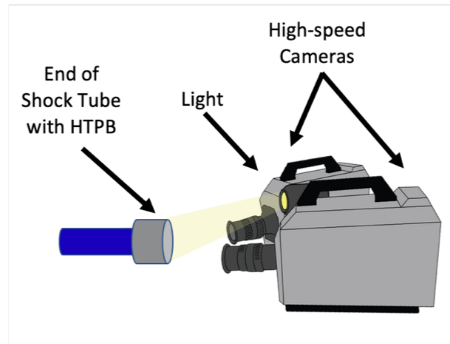

(b)

Figure 1: *(a) Computer-aided design (CAD) of the 7.62 cm (3-in.) diameter oxyacetylene shock tube, with 30.48 cm (1-ft) driver (red) and 457.2 (15-ft) driven (blue) section separated by a 1-mil thick Mylar diaphragm. Rupturing the Mylar by igniting the oxyacetylene in the driver creates a propagating shock wave through the driven section (see shock tube video: https://www.youtube.com/watch?v=5axDcOBtFMU). (b) The propagating shock wave will dynamically inflate the clamped inert HTPB sample and two high-speed cameras will record the deformation for 3D–DIC analysis.*

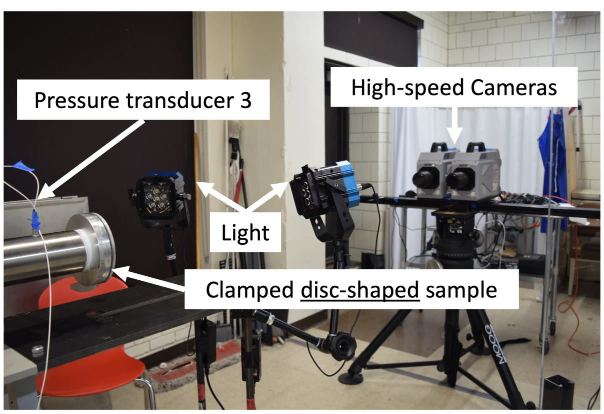

(a)

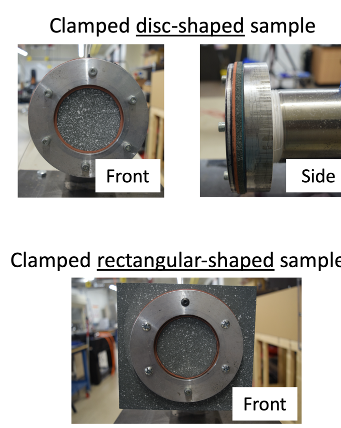

(b)

Figure 2: *(a) Experimental setup to facilitate 3D–DIC analysis of the clamped disc-shaped HTPB sample subjected to dynamic inflation. Pressure transducer 3 and the clamped sample are 15.24 cm (6-in.) apart. (b) Disc-shaped (top) and rectangular-shaped (bottom) HTPB sample that was clamped. The white dots on the surface are the speckles.*

2.3 Dynamic Tensile Elastic Modulus Calculation from Oxyacetylene-driven Shock tube Experiments

Deformation from the 3D–DIC analysis is used to quantify the phase velocity c of a propagating transverse strain wave on the propellant's surface, and also to calculate the angular frequency of vibration ω and dynamic tensile elastic modulus E, using the protocol described by [3]. Specifically, concepts from structural dynamics is applied to model HTPB as a thin plate under dynamic axisymmetric bending and vibration [19]. The dispersion relation $\omega = k^2\sqrt{\frac{D}{\rho h}}$ for propagating transverse waves in the HTPB plate, described in terms of ω and bending stiffness D, is applied. k is the wave number, ρ is the density of the HTPB sample, h is the plate thickness, and $D = \frac{Eh^3}{12(1-\nu^2)}$ with Poisson's ratio ν. Using concepts from thin plate bending analysis, the phase velocity $c = \frac{\omega}{k}$ is related to the wave number $k = \frac{3.1961}{a}$ rad/m for the clamped plate's fundamental mode, with plate radius a [3]. c is obtained from the DIC analysis by calculating the slope of the position of the maximum radial Green-Lagrange strain for different time points. Given c and k, ω is calculated and used to solve for E using the dispersion relation. The out-of-plane displacement W versus time t, at the HTPB apex or central point, is obtained from DIC analysis and is used to calculate the period T using the peak-to-peak out-of-plane displacement. The average time period T_{avg} of the peak-to-peak out-of-plane displacement is applied to calculate angular frequency $\omega = \frac{2\pi}{T_{avg}}$, as was done by [3]. Once ω is known, E can be solved using the dispersion relation in terms of the angular frequency and bending stiffness.

2.4 Inverse Finite Element Analysis (iFEA) to Extract Mechanical Properties

The commercially available softwares MATLAB and ABAQUS Explicit were coupled to perform the iFEA on disc-shaped samples with an assumed isotropic response for the HTPB material. A disc-shaped sample was utilized since the inner diameter of the annuli, used to clamp the samples, were sufficient to model the dynamic inflation experiments. The iFEA methodology to calibrate HTPB samples, modeled using either the linear elastic or linear viscoelastic properties, is shown in Figure 3.

Figure 4 shows the boundary and loading conditions, along with the mesh applied during the iFEA. A mesh convergence study was conducted to select the appropriate mesh size, which consisted of 3724 elements.

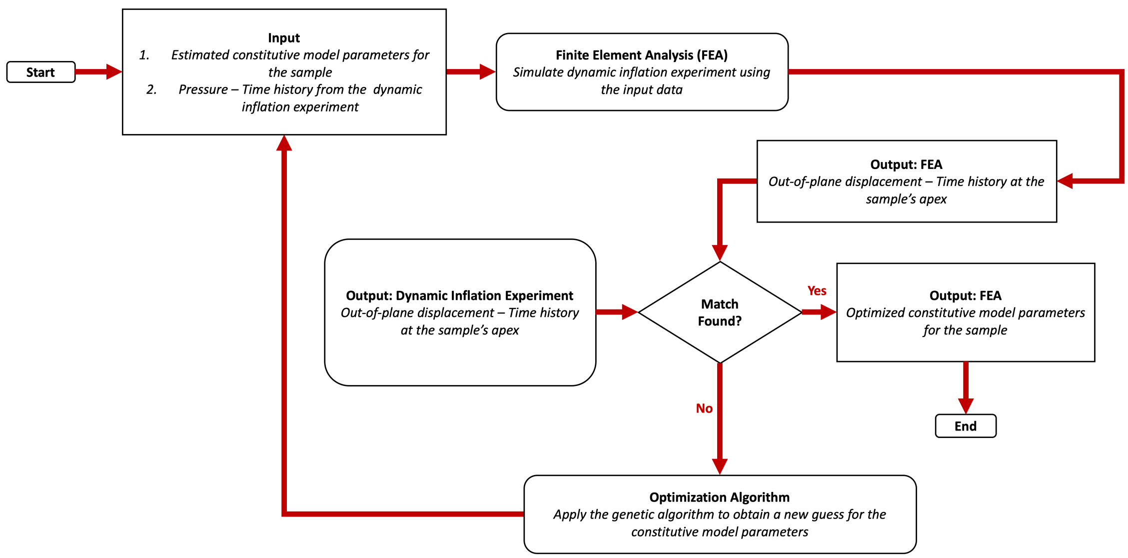

Figure 3: *Flowchart illustrating the iFEA methodology. MATLAB was used for the optimization using the built-in genetic algorithm function ga.*

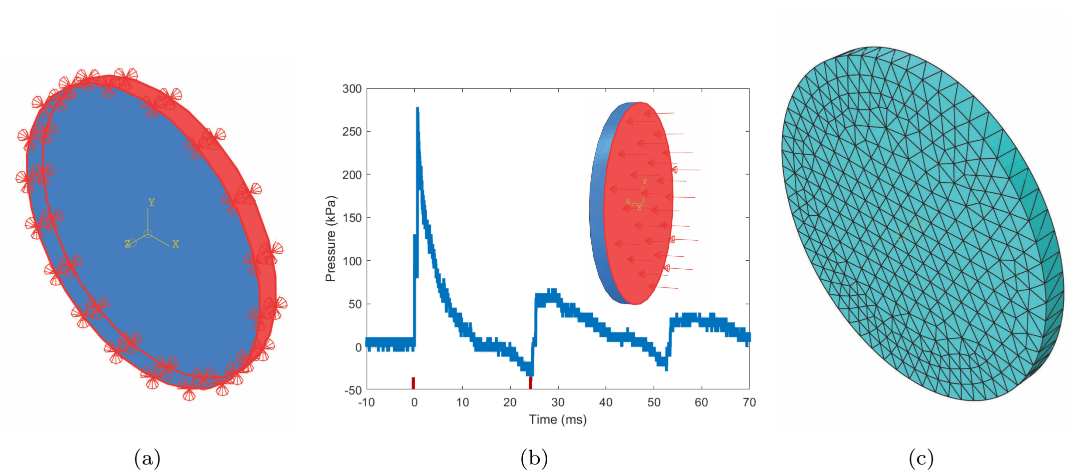

Figure 4: *(a) Fixed boundary condition (red) were applied around the circumference of the disc-shaped sample, to prevent translation in all directions. (b) The reflected pressure load, from pressure transducer 3 (Figure 2a), was applied on the circular cross-sectional area (red) of the sample (inset). The red tick marks denote the 0.25 ms time frame considered. (c) A 10-node modified quadratic tetrahedral mesh was used.*

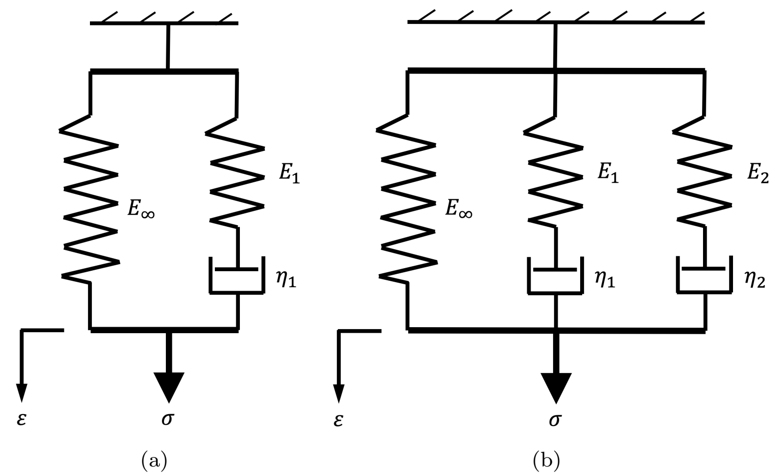

Figure 5: *Schematic of the generalized Maxwell model with (a) one Maxwell branch and (b) two Maxwell branches. The springs describe the elastic effects and the dashpot captures the viscous effects.*

When describing the HTPB as a linear elastic, the parameters that needed to be defined were the elastic modulus E and Poisson's ratio ν. A generalized Maxwell model, with either one or two Maxwell branches in parallel were used when characterizing the linear viscoelastic behavior of HTPB (Figure 5). The Maxwell branch consists of a spring and dashpot in series.

The relaxation modulus $E(t)$ of the system, which is essentially the Prony series, is defined in Equation 1 as [13]:

$$E\left(t\right) = E_0 - \sum_{i=1}^{N} E_i \left(1 - e^{-\frac{t}{\tau_i}}\right) \tag{1}$$

where $E_0 = E_\infty + \sum_{i=1}^{N} E_i$ is the instantaneous elastic modulus. E_∞ is the long-term (or equilibrium) elastic modulus and the relaxation time τ_i is obtained through the following relation: $\tau_i = \frac{\eta_i}{E_0}$, where η_i is the viscosity of the dashpot in Figure 5.

To implement the linear viscoelastic model, during the iFEA, a Prony series expansion in the time domain was expressed for both the shear modulus (Equation 2) and bulk modulus (Equation 3) [9].

$$G\left(t\right) = G_0 \left[1 - \sum_{i=1}^{N} g_i \left(1 - e^{-\frac{t}{\tau_i}}\right)\right] \tag{2}$$

where $G_0 = \frac{E_0}{2(1+\nu_0)}$ is the instantaneous shear modulus, g_i is the shear relaxation modulus ratio, and τ_i is the relaxation time. N represents the number of Maxwell branches in the Prony series.

$$K(t) = K_0 \left[1 - \sum_{i=1}^{N} k_i \left(1 - e^{-\frac{t}{\tau_i}} \right) \right] \tag{3}$$

where $K_0 = \frac{E_0}{3(1-2\nu_0)}$ is the instantaneous bulk modulus, k_i is the bulk modulus ratio, and τ_i is the relaxation time. N represents the number of Maxwell branches in the Prony series.

3 Results

3.1 Experiments: Dynamic Inflation

The oxyacetylene-driven shock tube was used to perform the dynamic inflation experiments by first sandwiching the samples in between two annuli plates, before clamping to the end of the shock tube. Table 2 provides values for the maximum reflected shock wave amplitude that was applied on the HTPB sample surface, the shock wave speed, and the dynamic tensile elastic modulus properties for HTPB sample numbers 3 – 7. An empty entry in Table 2 implies that 3D–DIC data could not be used to calculate the dynamic mechanical properties since the HTPB sample popped out of the annuli plate. Popping out was due to the magnitude of the reflected shock wave pressure applied on the surface and/or the high-speed cameras failing to record the event due to triggering by an acoustic trigger instead of pressure transducer 3. In the case where the cameras captured the samples popping out of the annuli plates, the shear wave speed c could be calculated using the time period prior to the samples popping out.

Reflected shock wave pressures with a maximum amplitude below 313 kPa did not cause the HTPB sample to pop out of the annuli plates. Figure 6 shows an example of the HTPB sample popping out of the annuli plates, due to the reflected shock wave pressures above 313 kPa.

Since the dynamic tensile elastic modulus E calculated using either ω or c were not comparable, for HTPB samples 5 and 7, the dynamic tensile elastic modulus was not calculated for the remaining samples. In Table 2, samples where the dynamic tensile elastic modulus was not calculated are labeled as “N/A”. The discrepancy between E, using either ω or c, is attributed to the HTPB sample behaving as a viscoelastic material, rather than an elastic material. Thus, thin plate bending analysis can not be applied. As a result, the iFEA was instead considered to extract the dynamic mechanical properties of HTPB (Section 3.2).

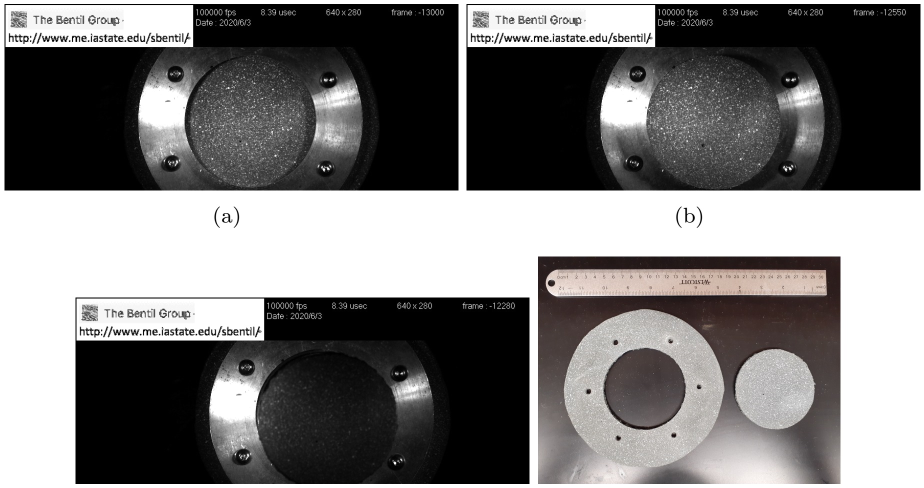

(a) (b)

(c) (d)

Figure 6: *(a) – (c) Time progression of a clamped HTPB sample popping out of the annuli plates from (a) time = 0 ms, (b) time = 4.5 ms, and (c) time = 7.2 ms. (d) Remnant of the HTPB sample (right), that popped out.*

Table 2: *Shock wave properties and calculated dynamic tensile elastic modulus. Not applicable (N/A) since there is discrepancy between the dynamic tensile elastic modulus magnitude calculated using angular frequency ω and the shear wave speed c.*

HTPB Sample Number	Reflected shock wave pressure on sample surface (kPa)	Shock wave speed via pressure transducers 2 and 3 (m/s)	Angular frequency ω (rad/s)	Shear wave speed c (m/s)	Dynamic tensile elastic modulus via ω (MPa)	Dynamic tensile elastic modulus via c (MPa)	3D-DIC Data?
HTPB Sample 1	323.63	408.03	-	-	-	-	No
HTPB Sample 2	471.26	454.93	-	-	-	-	No
HTPB Sample 3	369.06	423.33	-	24.180	-	23.299	No
HTPB Sample 4	334.99	413.01	-	24.235	-	22.8	No
HTPB Sample 5	278.21	392.78	1406.7	24.246	3.944	23.41	Yes
HTPB Sample 6	323.63	416.39	-	23.819	-	21.632	No
HTPB Sample 7	312.28	409.68	1540.0	24.156	4.637	22.798	Yes
HTPB Sample 8	258.34	373.53	-	-	-	-	No
HTPB Sample 9	309.44	388.78	-	-	-	-	No
HTPB Sample 10	105.04	337.17	N/A	N/A	N/A	N/A	Yes
HTPB Sample 11	190.21	368.12	N/A	N/A	N/A	N/A	Yes
HTPB Sample 12	241.31	375.37	N/A	N/A	N/A	N/A	Yes
HTPB Sample 13	229.95	381.00	N/A	N/A	N/A	N/A	Yes
HTPB Sample 14	218.59	381.00	N/A	N/A	N/A	N/A	Yes
HTPB Sample 15	235.63	382.91	N/A	N/A	N/A	N/A	Yes

3.2 iFEA: Dynamic Inflation

Table 3 and Table 4 show the parameters provided for the linear elastic and linear viscoelastic properties in ABAQUS Explicit, respectively.

Table 3: *Linear elastic constitutive model parameters. The term "optimized" implies that the genetic algorithm was used to optimize the value of the parameter.*

Parameter	Value
Elastic modulus E (Pa)	17,311,837 *(optimized)*
Poisson's ratio ν	0.49
Density ρ (kg/m^3)	2181.5

Table 4: *Linear viscoelastic constitutive model parameters. The term "optimized" implies that the genetic algorithm was used to optimize the value of the parameter.*

Parameter	Value
Instantaneous Poisson's ratio ν_0	0.49
Density ρ (kg/m^3)	2181.5
Prony Series – One Maxwell Branch	
Instantaneous elastic modulus E_0 (Pa)	28,178,076 *(optimized)*
g_1	0.9434 *(optimized)*
k_1	0.6462 *(optimized)*
τ_1 (s)	0.0014 *(optimized)*
Prony Series – Two Maxwell Branches	
Instantaneous elastic modulus E_0 (Pa)	14,100,695 *(optimized)*
g_1	0.0746 *(optimized)*
k_1	0
τ_1 (s)	0.0070 *(optimized)*
g_2	0.7928 *(optimized)*
k_2	0
τ_2 (s)	8.6387×10^{-4} *(optimized)*

Figure 7 compares the contour plots from DIC and iFEA, using the optimized parameters from the Prony series with the two Maxwell branches.

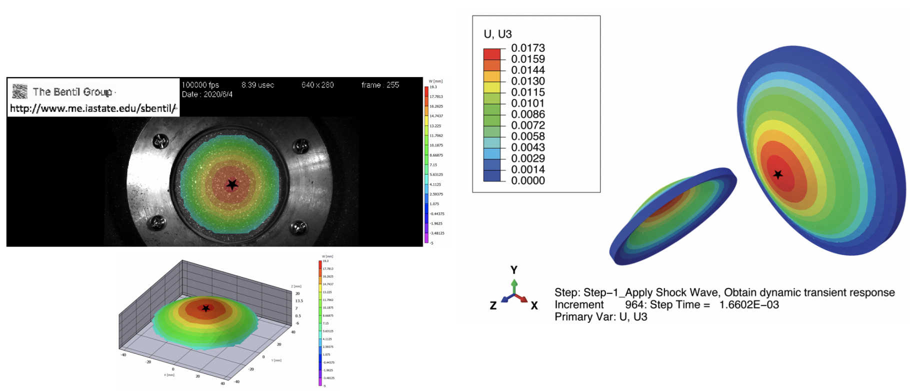

(a) (b)

Figure 7: *Out-of-plane displacement W at the apex, which is denoted by the star from (a) DIC and (b) iFEA.*

Figure 8 compares the results of DIC and iFEA, using the optimized parameters from the linear elastic and linear viscoelastic constitutive models.

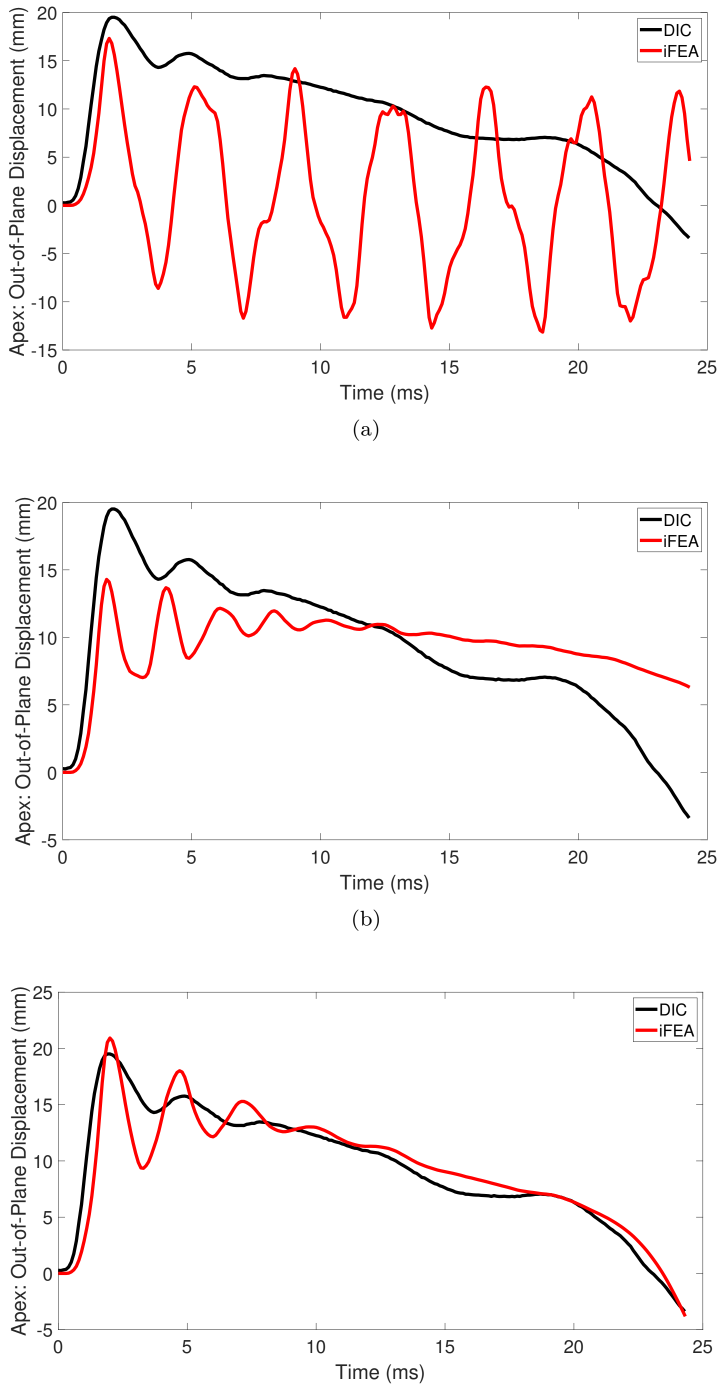

Figure 8: *Out-of-plane displacement W at the apex from DIC (black) and iFEA (red) for (a) linear elastic and Prony series with (b) one Maxwell branch and (c) two Maxwell branches.*

4 Discussion & Conclusion

HTPB samples were exposed to shock waves during a dynamic inflation experiment, to characterize the mechanical properties at high strain rates. During the experiment, 3D-DIC was applied to capture the surface deformation of the HTPB samples. Concepts from thin plate bending theory was initially applied to calculate the dynamic tensile elastic modulus E, using both the angular frequency of vibration ω and the phase velocity c of a propagating transverse strain wave on the propellant's surface. Ideally, E calculated using either ω or c should be comparable. However, this was not the case due to the material properties of HTPB. As an alternative, an iFEA was applied to predict the material properties of HTPB by considering a linear elastic and linear viscoelastic constitutive model. The linear elastic model was chosen to determine how well the predicted E from iFEA compared with the E calculated using ω and c. For HTPB sample 5, the predicted E from iFEA was 126% and 30% different, when compared with E calculated using ω and c, respectively.

A linear viscoelastic model comprised of a Prony series with two Maxwell branches provided a better fit with the 3D–DIC data than one with one Maxwell branch. Future iFEA simulations will consider additional Maxwell branches to improve the fit with the 3D–DIC data, to best characterize the HTPB's mechanical properties.

References

[1] A Ajovalasit and B Zuccarello. Local reinforcement effect of a strain gauge installation on low modulus materials. *The Journal of Strain Analysis for Engineering Design*, 40(7):643–653, April 2005.

[2] E. Alay, M. Skotak, A. Misistia, and N. Chandra. Dynamic loads on human and animal surrogates at different test locations in compressed-gas-driven shock tubes. *Shock Waves*, 28(1):51–62, January 2018.

[3] S. A. Bentil, K. T. Ramesh, and T. D. Nguyen. A Dynamic Inflation Test for Soft Materials. *Experimental Mechanics*, 56(5):759–769, June 2016.

[4] Brad L. Boyce, J. Mark Grazier, Reese E. Jones, and Thao D. Nguyen. Full-field deformation of bovine cornea under constrained inflation conditions. *Biomaterials*, 29(28):3896–3904, October 2008.

[5] S L Evans and C A Holt. Measuring the mechanical properties of human skin in vivo using digital image correlation and finite element modelling , Measuring the mechanical properties of human skin in vivo using digital image correlation and finite element modelling. *The Journal of Strain Analysis for Engineering Design*, 44(5):337–345, July 2009.

[6] Mikko Hokka, Nikolas Mirow, Horst Nagel, Marc Irqsusi, Sebastian Vogt, and Veli-Tapani Kuokkala. In-vivo deformation measurements of the human heart by 3D Digital Image Correlation. *Journal of Biomechanics*, 48(10):2217–2220, July 2015.

[7] Mohammad Hosseini-Farid, Mohammadreza Ramzanpour, Mariusz Ziejewski, and Ghodrat Karami. A compressible hyper-viscoelastic material constitutive model for human brain tissue and the identification of its parameters. *International Journal of Non-Linear Mechanics*, 116:147–154, November 2019.

[8] M. Kauer, V. Vuskovic, J. Dual, G. Szekely, and M. Bajka. Inverse finite element characterization of soft tissues. *Medical Image Analysis*, 6(3):275–287, September 2002.

[9] Kathryn E. Keenan, Saikat Pal, Derek P. Lindsey, Thor F. Besier, and Gary S. Beaupre. A viscoelastic constitutive model can accurately represent entire creep indentation tests of human patella cartilage. *Journal of Applied Biomechanics*, 29(3):292–302, June 2013.

[10] Le Anhduong Q., Sun L. Z., and Miller Timothy C. Health Monitoring and Diagnosis of Solid Rocket Motors with Bore Cracks. *Journal of Aerospace Engineering*, 29(3):04015058, May 2016.

[11] V. Libertiaux, F. Pascon, and S. Cescotto. Experimental verification of brain tissue incompressibility using digital image correlation. *Journal of the Mechanical Behavior of Biomedical Materials*, 4(7):1177–1185, October 2011.

[12] Giacomo Lionello and Luca Cristofolini. A practical approach to optimizing the preparation of speckle patterns for digital-image correlation. *Measurement Science and Technology*, 25(10):107001, October 2014.

[13] R. Michalczyk. Implementation of generalized viscoelastic material model in ABAQUS code. *Logistyka*, (nr 6), 2011.

[14] Timothy C. Miller. Poisson's Ratio Extrapolation from Digital Image Correlation Experiments. Technical Report AFRL-RQ-ED-TP-2013-154, AIR FORCE RESEARCH LAB EDWARDS AFB CA ROCKET PROPULSION DIV, March 2013.

[15] Timothy C. Miller. Damage and Dilatometry for Solid Propellants with Digital Image Correlation. *Propellants, Explosives, Pyrotechnics*, 44(2):234–245, 2019.

[16] Kristin M. Myers, Baptiste Coudrillier, Brad L. Boyce, and Thao D. Nguyen. The inflation response of the posterior bovine sclera. *Acta Biomaterialia*, 6(11):4327–4335, November 2010.

[17] Sebnem Ozupek and Eric B. Becker. Constitutive Equations for Solid Propellants. *Journal of Engineering Materials and Technology*, 119(2):125–132, April 1997.

[18] Marco Palanca, Gianluca Tozzi, and Luca Cristofolini. The use of digital image correlation in the biomechanical area: A review. *International Biomechanics*, 3(1):1–21, January 2016.

[19] J. S. Rao. *Dynamics of Plates J.S. Rao.* Number Book, Whole. Marcel Dekker ;New Delhi, New York, 1999.

[20] G. Subhash, Q. Liu, D. F. Moore, P. G. Ifju, and M. A. Haile. Concentration Dependence of Tensile Behavior in Agarose Gel Using Digital Image Correlation. *Experimental Mechanics*, 51(2):255–262, February 2011.

[21] MA Sutton, Cheng Mingqi, WH Peters, YJ Chao, and SR McNeill. Application of an optimized digital correlation method to planar deformation analysis. *Image and Vision Computing*, 4(3):143–150, August 1986.

[22] Michael A. Sutton, Jean Jose Orteu, and Hubert Schreier. *Image Correlation for Shape, Motion and Deformation Measurements: Basic Concepts,Theory and Applications*. Springer US, 2009.

[23] Kyeong-Soo Yun, Jae-Beom Park, Gyoo-Dong Jung, and Sung-Kie Youn. Viscoelastic constitutive modeling of solid propellant with damage. *International Journal of Solids and Structures*, 80:118–127, February 2016.

[24] Dongsheng Zhang and Dwayne D. Arola. Applications of digital image correlation to biological tissues. *Journal of Biomedical Optics*, 9(4):691–699, 2004 Jul-Aug.